Mon. Not. R. Astron. Soc. **299,** 467–478 (1998)

MERLIN polarization observations of compact steep-spectrum sources at 5 GHz

E. Lüdke,[1⋆] S. T. Garrington,[1] R. E. Spencer,[1] C. E. Akujor,[1,2,3] T. W. B. Muxlow,[1] H. S. Sanghera[1,4] and C. Fanti[5]

[1]*The University of Manchester, Nuffield Radio Astronomy Laboratories, Jodrell Bank, Cheshire SK11 9DL*
[2]*School of Physical Sciences, PMB 2000, Imo State University, Owerri, Imo State, Nigeria*
[3]*Max-Planck Institut für Radioastronomie, Auf dem Hügel 69, Bonn D-5300, Germany*
[4]*Radiosterrenwacht Dwingeloo, Postbus 2, Dwingeloo NL-7990, The Netherlands*
[5]*Istituto di Radioastronomia del CNR, Via Gobetti 101, 40129, Bologna, Italy*

Accepted 1998 May 1. Received 1998 April 8; in original form 1994 September 7

ABSTRACT

We present polarization observations of 28 compact steep-spectrum sources made with the upgraded MERLIN at 5 GHz. With an angular resolution of 60 milliarcsec and rms noise levels of about 0.1 mJy beam^{-1}, the total intensity images reveal new details in many of these sources. A few of the more extended lobes and jets are quite highly polarized, but more than half of the components are completely unpolarized. Comparison with published data implies that this is due to Faraday depolarization, probably occurring in the surrounding medium with $nB \sim 1$ cm^{-3} μG. The high resolution of the present observations implies that the variations in Faraday rotation, probably due to magnetic field tangling, occur on scales of less than about 100 pc.

Key words: polarization – techniques: miscellaneous – galaxies: ISM – galaxies: jets – radio continuum: galaxies.

1 INTRODUCTION

Compact steep-spectrum (CSS) sources are objects with intrinsically small (subgalactic) linear sizes and steep integrated synchrotron spectra, $\alpha \geq 0.5$ ($S_\nu \propto \nu^{-\alpha}$). Their small sizes are not thought to be due to significant projection effects (Fanti et al. 1990). It has been debated whether these sources are simply young, or are confined to small sizes, perhaps by a denser interstellar medium (ISM) in their host galaxies (Fanti et al. 1995; Readhead et al. 1996). Information on the ages and environments of the sources, provided by multi-frequency radio observations using spectral index and polarization measurements, can be used to help distinguish between these possibilities.

In particular, high-resolution polarization mapping is a powerful tool for studying the properties of the ISM as well as the magnetic field geometry and physical conditions in the source. The 1991 upgrade to the MERLIN array (Thomasson 1986; Wilkinson 1991) makes the instrument ideally suited for the measurement of polarization at high resolution.

In this paper we briefly discuss technical aspects of polarization observations with the upgraded MERLIN, present maps of 28 CSS sources, and discuss their polarization properties.

⋆ Present address: UFSM/NEPAE-Centro de Tecnologia, Santa Maria-RS-97119, Brazil.

2 OBSERVATIONS AND DATA REDUCTION

Before the recent upgrade, polarization measurements with MERLIN were limited by the number of correlator channels available and the fact that the microwave links returned only one hand of polarization at a time from each telescope, necessitating a complex switching cycle. As a result, early polarization experiments with MERLIN were restricted to observations of sources with strong polarized flux density like 3C 273 (Flatters & Conway 1985) and 3C 380 (Flatters 1987).

The new 5-GHz system comprises six antennas (Tabley, Darnhall, Mark II, Knockin, Defford and the new 32-m telescope at Cambridge) equipped with low-noise cryogenic HEMT receivers with simultaneous dual-polarization capabilities. At the band centre of 4993 MHz, the system temperatures for the MERLIN telescopes are 35 K on average (55 K at Defford). The signals are brought from each antenna by AM microwave links adapted to carry both hands of circular polarization (L,R) at 16-MHz maximum bandwidth each. The parallel (LL,RR) and cross-correlations (RL,LR) are formed in a 2-bit digital correlator followed by Fourier transformation to give 15×1 MHz frequency channels. These improvements allow high-sensitivity polarization maps to be produced with a maximum resolution of ∼40 mas at 5 GHz, and with rms noise levels of ∼75 μJy beam^{-1} after a 12-h track.

The sample of CSS sources studied here follows the criteria of Fanti et al. (1990), and consists of all sources in the 3C R catalogue (Jenkins, Pooley & Riley 1977) with projected linear sizes less than 15 kpc (for H_0=100 km s^{-1} Mpc^{-1} and q_0=0.5) and high-frequency (> 1 GHz) spectral indices steeper than 0.5. Of the 30 sources listed by Fanti et al., we have omitted the smallest source (3C 287) which would be completely unresolved by MERLIN, one source which turns out to be one-half of an asymmetric double (3C 299), and one source with extended lobes (3C 346); a further source (3C 455) was not observed because of scheduling problems. Two sources have been added to this list: 3C 258 fell just below the flux density limit of 3C R, and 4C 13.66 was included in the revised 3C sample of Laing, Riley & Longair (1983).

Most of the sources (Table 1) were observed for a full track of at least 12 h. In a few cases, two nearby sources were interleaved (3C 303.1/3C 305.1 and 3C 343/3C 343.1). Phase calibrator sources, chosen from the VLA Calibrator List or the MERLIN Calibrator List (Patnaik et al. 1992) were observed for 2–3 min in every 10 min. Initial calibration, including correction for amplitude and phase variations across the 15-MHz band, was derived from daily observations of unresolved sources (0552+398 or OQ 208) whose flux densities were derived by comparison with 3C 286, for which a flux density of 7.26 Jy was used (Baars et al. 1977). The overall flux density calibration should be accurate to 5 per cent.

Having averaged the data to a single 15-MHz band, the phase calibrator was mapped using 3 cycles of self-calibration, and the corrections were applied to both target source and calibrator by interpolation. At this stage, polarization leakage terms were derived by using the parallactic angle method (Conway & Kronberg 1969). Here, the phase calibrators at declinations > 10° have good parallactic angle coverage, and were used to derive telescope polarization crosstalk, or '*D*-terms' (Bignell & Perley 1985) by solving simultaneously for the polarization characteristics of the calibrator and telescope feed crosstalk. The instrumental polarization has been shown to be constant over a week (Lüdke 1994). For some sources at lower declinations the '*D*-terms' from the nearest run on a high-declination source were applied. The polarization corrections were applied back to the phase calibrator to assess the calibration quality. On average, $|D| \leq 3$ per cent, and the amplitude and the polarization calibration were accurate to 0.5 per cent. The polarization position angle was calibrated using the short daily observations of 3C 286, for which a position angle of 33° was assumed.

The phase-calibrated images were refined using several cycles of self-calibration. In some cases the DIFMAP program was used for this stage of the processing. After mapping the target source with about 10 cycles of self-calibration, the maps of the Stokes parameters I, Q and U were produced. The final maps of polarization position angle $[\chi = (1/2)\tan^{-1}(U/Q)]$ and percentage polarization ($m = 100\sqrt{Q^2 + U^2}/I$) were made.

The initial phase calibration means that the astrometry of the images is accurate to 20 mas, in the extragalactic radio reference frame.

Maps of the sources at 6 cm are presented in Fig. 1. In practice, the resolution varies with the source declination. To keep uniformity, the maps presented in Fig. 1 were convolved to a standard circular beam of 50–65 mas FWHM. Sources have been decomposed into bright subcomponents, and their polarization measurements are given in Table 2.

Table 1. Observational parameters and journal of observations. Largest angular sizes (*LAS*), largest linear sizes (*LLS*) and optical identification (G = galaxy, Q = quasar) are given. This table also gives the lowest contour for each of the maps in Fig. 1, along with the scale for the polarization vectors as the percentage polarization represented by a vector 1 arcsec long.

Name	z	Id	LAS arcsec	S_{peak} mJy/beam	*LLS* kpc	ϕ-cal.	Obs. date	Lowest contour mJy/beam	Pol. scale per cent/arcsec
3C 43	1.47	Q	2.6	320	11.1	0149+218	920614	1.7	500
3C 48	0.37	Q	1.3	870	4.0	0202+319	920615	9.0	333
3C 49	0.62	G	1.0	730	3.8	0119+115	921208	0.5	
3C 67	0.31	G	2.5	126	7.0	0234+285	920527	0.5	250
3C 93.1	0.24	G	0.2	423	0.5	0424+414	950709	1.5	5000
3C 119	0.41	G	0.2	2962	0.75	0424+414	950709	5.0	50
3C 138	0.76	Q	0.8	1091	3.3	0528+134	920710	8.0	333
3C 147	0.54	Q	0.7	67	2.63	0532+506	921105	2.5	500
3C 186	1.06	Q	1.2	32	5.1	0739+398	920807	0.3	
3C 190	1.21	Q	2.6	65	11.2	0748+126	920615	0.5	
3C 216	0.67	Q	1.5	671	5.9	0917+449	920620	1.0	500
3C 237	0.88	G	1.3	271	5.6	1005+066	950617	1.0	67
3C 241	1.62	G	1.2	112	5.1	1013+208	921206	1.2	
3C 258	0.17	G	0.10	206	0.2	1119+183	950626	0.75	
3C 268.3	0.37	G	1.3	161	4.0	1226+638	920506	0.5	333
3C 277.1	0.32	Q	1.6	171	4.6	1300+580	950418	0.3	500
3C 286	0.85	Q	3.8	5948	15.8	1308+326	920518	4.0	500
3C 298	1.44	Q	1.5	279	6.3	1408+077	950505	0.75	333
3C 303.1	0.27	G	1.9	21	4.8	1448+762	950530	0.4	208
3C 305.1	1.13	G	10.1	42	10.1	1448+762	950530	0.4	200
3C 309.1	0.90	Q	2.2	1681	9.2	1531+722	920727	2.5	500
3C 318	0.75	G	0.8	288	3.2	1511+238	920616	3.0	500
3C 343	0.99	Q	0.15	423	0.6	1634+604	950629	1.0	133
3C 343.1	0.75	G	0.24	385	1.0	1634+604	950629	1.5	
3C 380	0.69	Q	1.5	2980	5.9	1851+488	921228	3.0	500
3C 454	1.76	Q	0.6	231	2.5	2246+208	921106	0.75	500
3C 454.1	1.84	G	1.60	97	6.66	2251+704	950703	0.3	
4C 13.66	1.45	G	1.2	118	5.1	1749+096	920808	0.75	

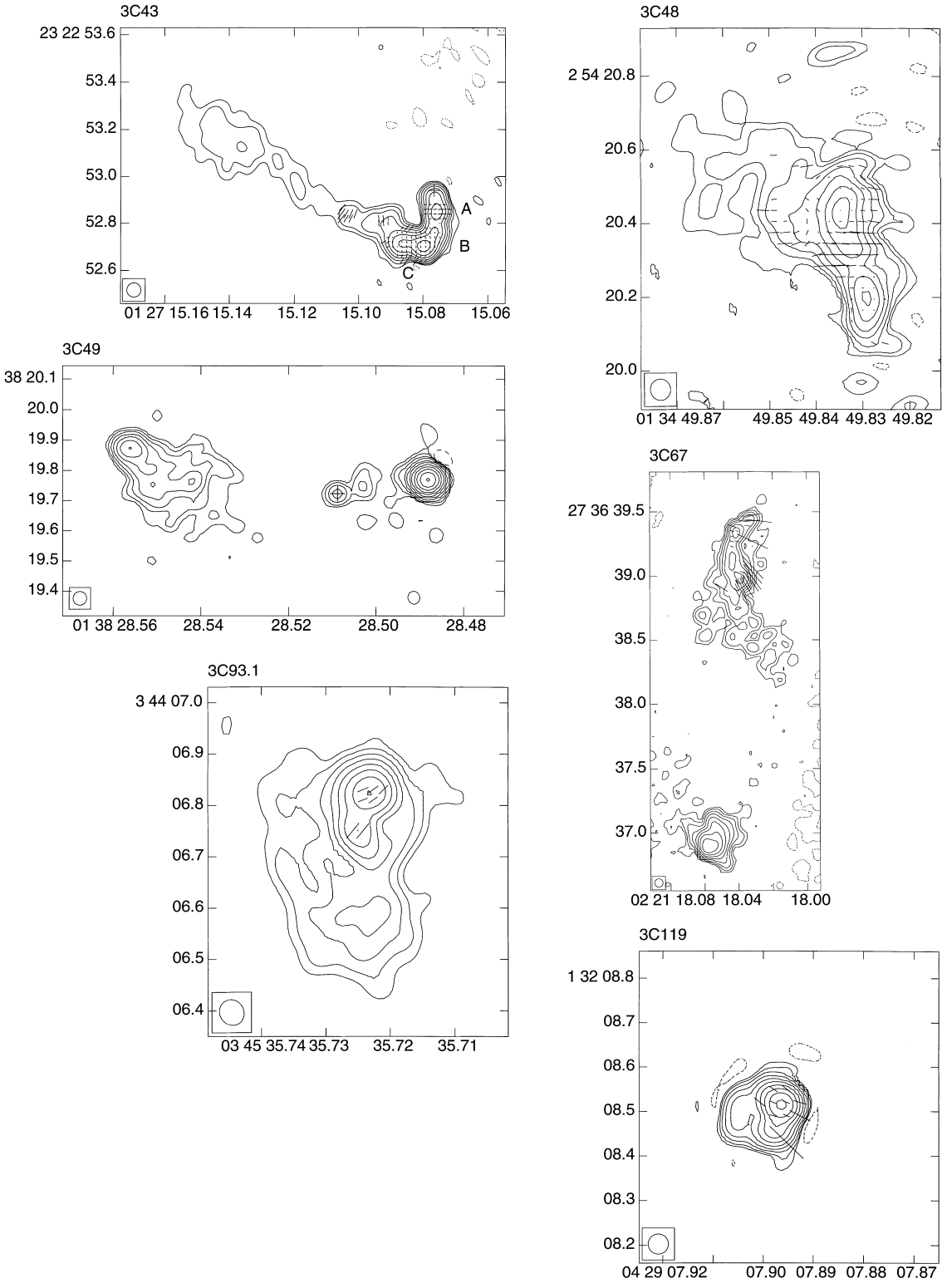

Figure 1. MERLIN maps of CSS sources. The contour levels are logarithmically spaced by a factor of 2. The lowest contours are given in Table 1. The polarization vectors show the direction of the observed electric field and have lengths proportional to the fractional polarization, with a scaling factor given in Table 1. Core components discussed in the text are marked with a cross. Map coordinates are equinox 1950.

Some of the sources were observed jointly as part of another programme, and total intensity images of these have been published by Sanghera et al. (1995). All the images are included here for completeness.

3 COMMENTS ON INDIVIDUAL SOURCES

3C 43. The structure of this source has been discussed by Akujor, Spencer & Saikia (1991), and EVN+MERLIN images at 1.6 GHz

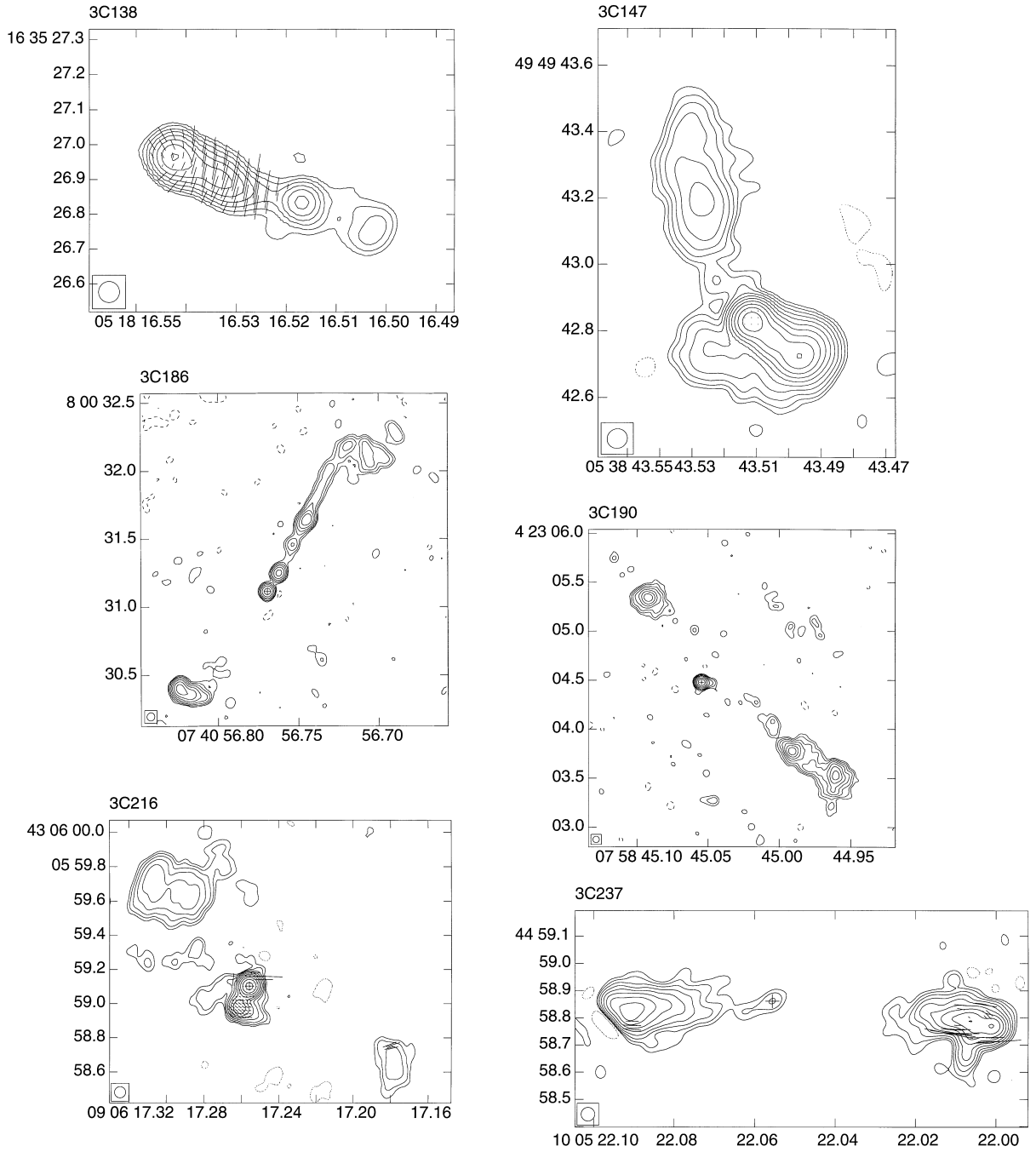

Figure 1 – *continued*

have been presented by Spencer et al. (1991). The MERLIN 5-GHz image shown here shows the inner, bent jet and its extension towards the diffuse eastern lobe. By applying a Gaussian taper to the original 1.6-GHz EVN data of Spencer et al., a map convolved to 60 mas has been obtained and used to derive the spectral index along the jet. Hence the core of this source at the position labelled in Fig. 1 ($01^{\rm h}27^{\rm m}15\overset{\rm s}{.}077$, $23°22'52\overset{''}{.}94$) has $\alpha \leq 0.2$, while the brightest component has $\alpha \sim 0.3$. The northern component seen by Spencer et al. with $S_I \sim 62$ mJy was also detected at a low signal-to-noise ratio, but it has been excluded from the figure in order to display the polarization vectors more clearly.

The pattern of polarization vectors in similar to the pattern at 15 GHz (van Breugel et al. 1992), implying little Faraday rotation at 5 GHz, and therefore the magnetic field follows the direction of the curved jet.

3C 48. A detailed EVN+MERLIN image has been made by Wilkinson et al. (1991), who discuss the structure of this source in terms of a disrupted jet. In the MERLIN 5-GHz image, almost all of the polarized emission comes from the inner part of the northern component, where the fractional polarization reaches 9 per cent. By comparison with the 15-GHz image of van Breugel et al. (1992), there may be significant Faraday rotation in the northern part of the source. Higher resolution polarization observations are needed to enable further interpretation.

3C 49. The MERLIN 5-GHz image confirms that the central component at $01^{\rm h}38^{\rm m}28\overset{\rm s}{.}509$, $13°38'19\overset{''}{.}73$ is indeed the core:

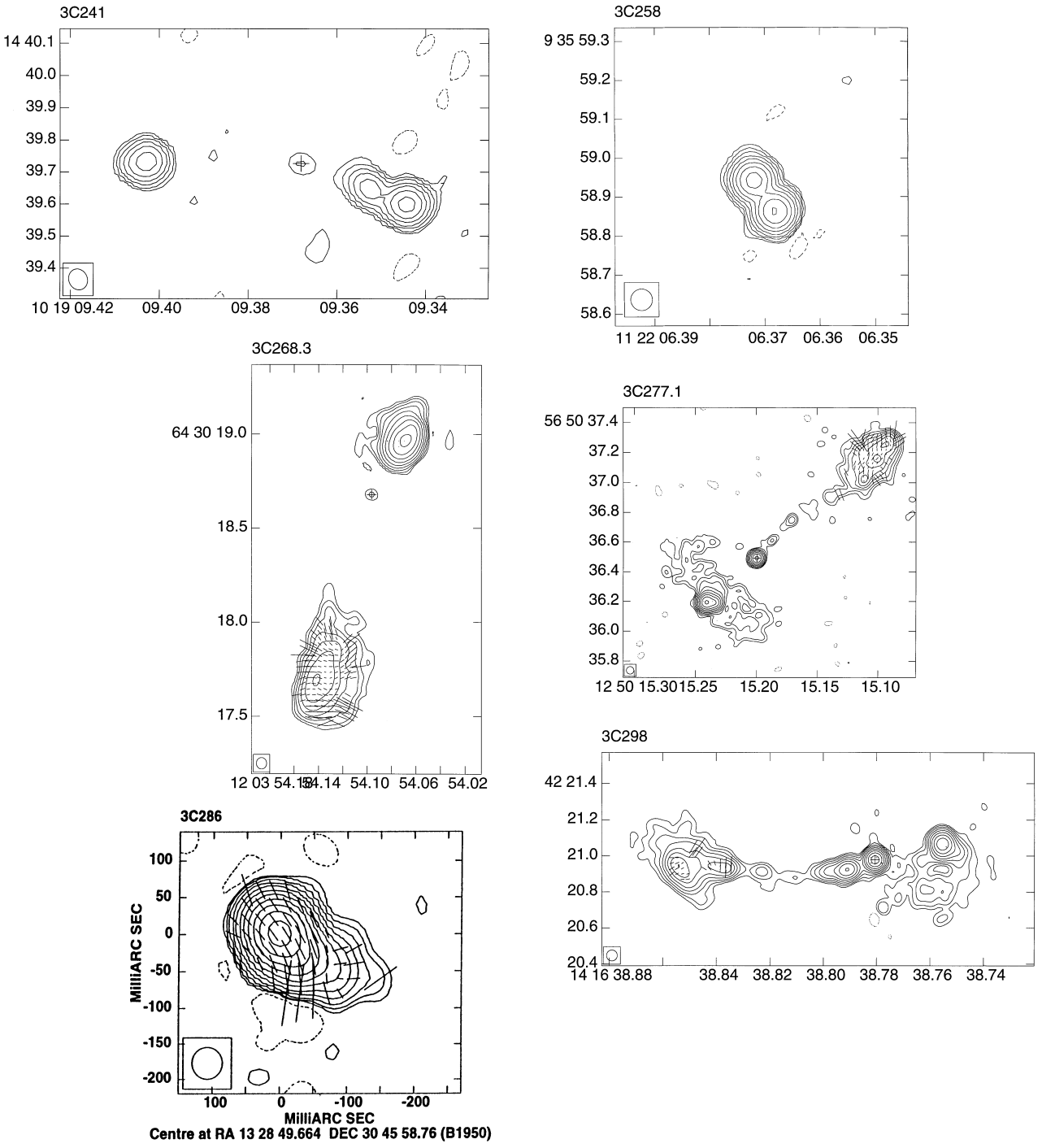

Figure 1 – *continued*

comparison with the 15-GHz image of van Breugel et al. (1992) gives $\alpha = 0.1 \pm 0.1$. A jet is seen linking this core to the bright western hotspot. No polarization is detected at 5 or 15 GHz, although there may be a marginal detection of polarized emission at the 1 per cent level in the western hotspot (Akujor & Garrington, in preparation).

3C 67. This radio galaxy is very asymmetric in both radio structure and polarization. The extended northern lobe shows high polarization in the MERLIN 5-GHz image, and comparison with the 15-GHz image of van Breugel et al. (1992) shows very little depolarization or Faraday rotation between 5 and 15 GHz. The polarization vectors in the MERLIN image show that the magnetic field is parallel to the boundary of the radio lobe, as is common in more extended sources. In contrast, the southern lobe is brighter, more compact, and unpolarized at both 5 and 15 GHz. The map presented by Sanghera et al. (1995), made from a longer, independent observation without polarization information, shows a possible weak core about 0.6 arcsec north of the peak in the southern component. The flux density of this core is 1.5 ± 0.5 mJy, just at the detection threshold of the map presented here.

3C 93.1. The new MERLIN map shows that this source shows a compact component with a possible jet to the south, surrounded by

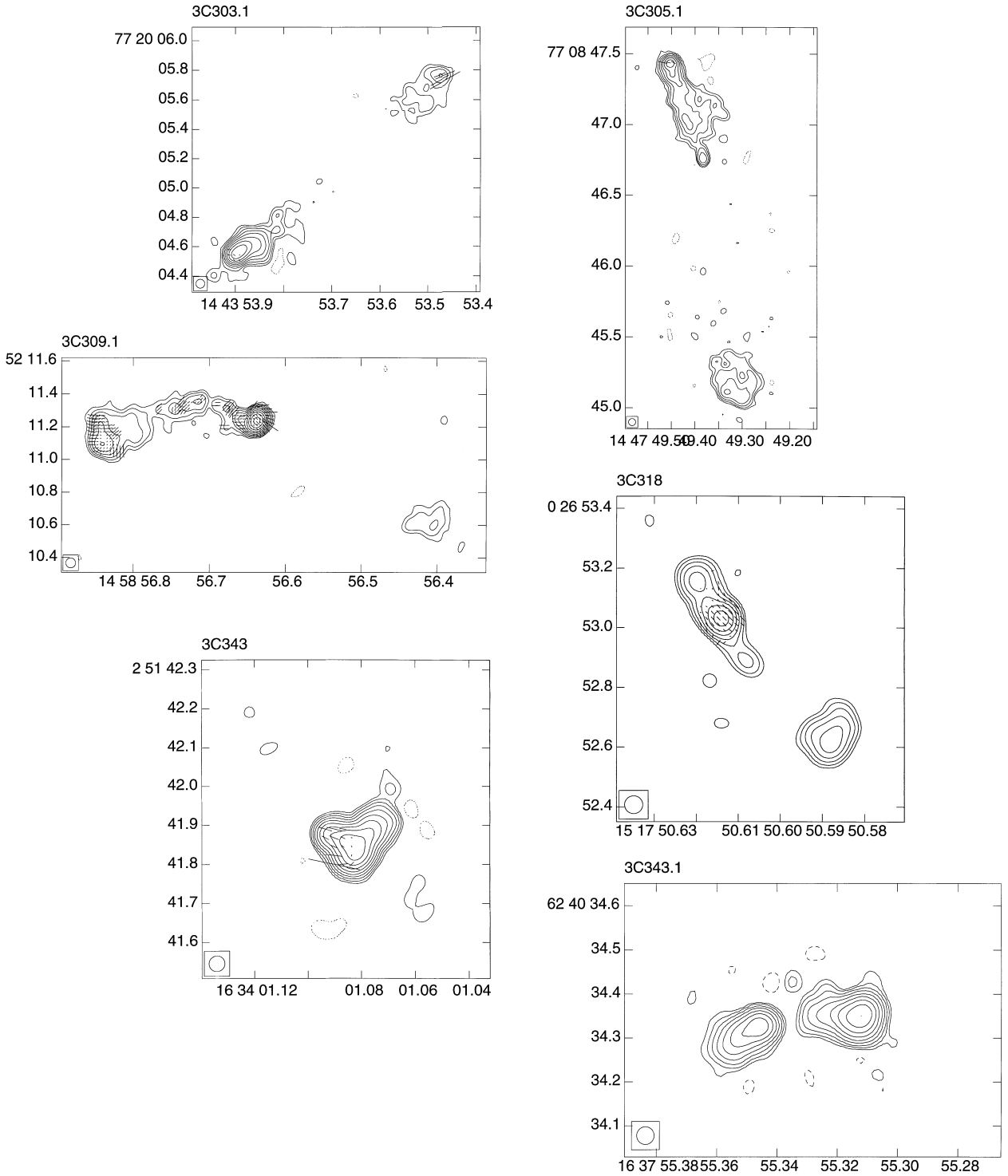

Figure 1 – *continued*

some diffuse emission. VLBI observations (Dallacasa et al. 1990) also reveal a compact feature surrounded by diffuse emission.

3C 119. The complex spiral structure of this source has been discussed in detail by Ren-dong et al. (1991), but the MERLIN image barely resolves it. This source shows extremely rapid depolarization between 8.4 GHz, where the integrated fractional polarization is 8.5 per cent (Browne, private communication), and 5 GHz, where the polarization has fallen to less than 1 per cent.

3C 138. The structure of the quasar, which consists of a core with a bright jet and hotspot to the east and a fainter, more diffuse lobe to the west, has been discussed by Akujor et al. (1993). Polarization images at 8.4, 15 and 22 GHz have been presented by Akujor & Garrington (1995), van Breugel et al. (1992) and Akujor et al. (1993), and a VLBI polarization image at 5 GHz has been made by Dallacasa et al. (1995). The average polarization of the jet and hotspot increases slightly from 12 per cent at 5 GHz to 14 per cent at 15 GHz. Locally, the polarization of the jet increases to 25 per cent near the core at 15 and 22 GHz, but at 5 GHz with similar

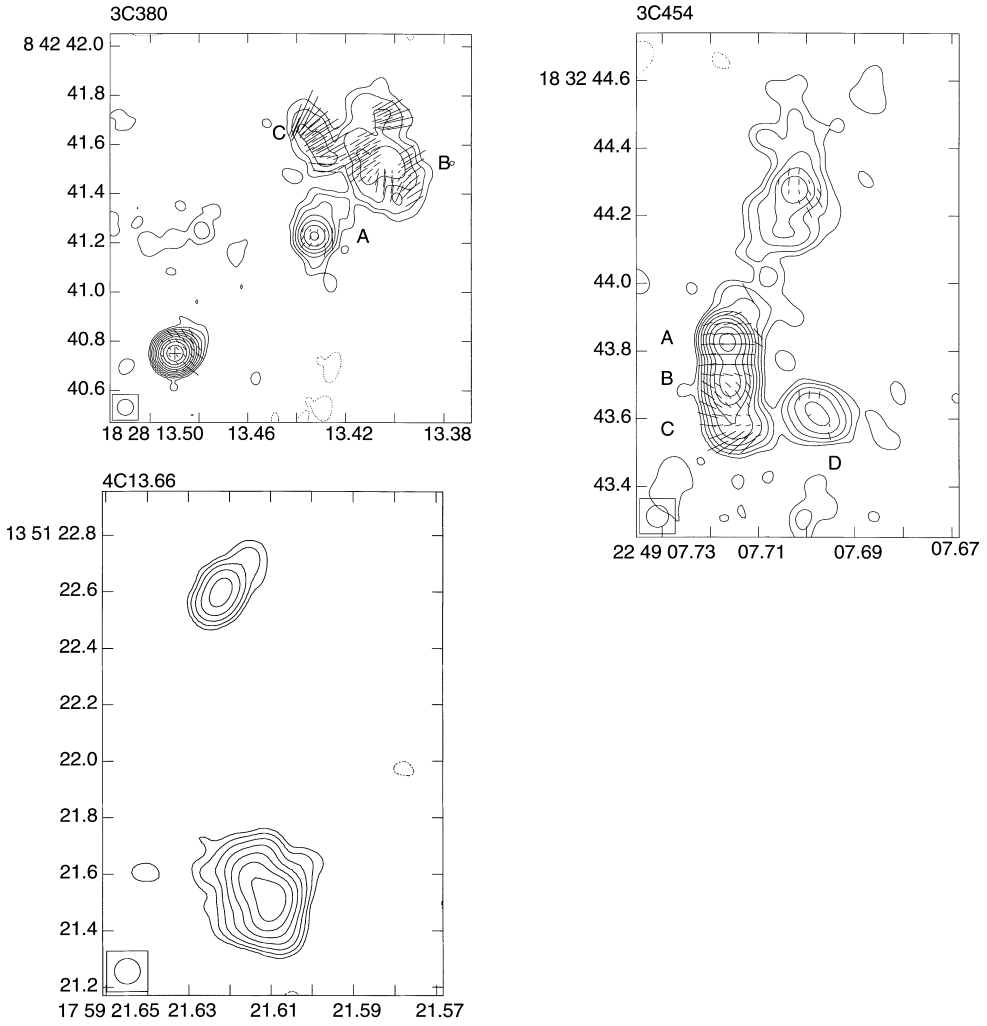

Figure 1 – *continued*

resolution the polarization is only 15–20 per cent in the MERLIN image. This may indicate some depolarization of the jet near the core.

3C 147. The total intensity structure of this quasar has been studied in detail by MERLIN (Akujor, Spencer & Wilkinson 1990) and the EVN (Zhang et al. 1991). The new MERLIN 5-GHz map shows the diffuse northern lobe and the jet to the south-west of the core, surrounded by diffuse emission. The source is barely polarized at 5 GHz, but VLA images at 8.4 and 15 GHz (Akujor & Garrington 1995) show significant polarization in the northern lobe, indicating that this lobe is depolarized at 5 GHz.

3C 186. MERLIN and EVN images at 1.6 GHz have been presented by Spencer et al. (1991), who found a fragmented one-sided jet in this source. The new MERLIN 5-GHz image confirms the location of the core at $07^{\rm h}40^{\rm m}56\overset{\rm s}{.}769$, $38°00'31\overset{''}{.}11$, with very similar flux densities at 15, 5 and 1.6 GHz. At 60-mas resolution, the MERLIN image shows that the jet is remarkably straight and smooth between the knot and the hotspot. The southern lobe, on the other hand, appears to be bent at 90° from the source axis. No polarization is detected in the MERLIN 5-GHz image.

3C 190. This source has been mapped using the EVN and MERLIN by Spencer et al. (1991). We confirm the location of the flat-spectrum core at $07^{\rm h}58^{\rm m}45\overset{\rm s}{.}055$, $14°23'04\overset{''}{.}48$ by comparison with 15- and 1.6-GHz images. The MERLIN 5-GHz image confirms that the jet emerges initially to the west from the core, exhibiting an almost right-angle bend. At 5 GHz no polarization is detected in the MERLIN image, but at 15 GHz the polarization of the jet rises to 10 per cent (van Breugel et al. 1992), indicating strong depolarization at 5 GHz. The bright northern lobe is unpolarized at both 5 and 15 GHz. More extended emission to the south of the jet has been seen at lower resolution (Pearson, Readhead & Perley 1985; Spencer et al. 1991).

3C 216. This quasar has complex structure on arcsecond and milliarcsecond scales (Fejes, Porcas & Akujor 1992). The MERLIN image presented here shows the flat spectrum core and the jet to the south-east, which then bends abruptly to the west. The inner part of this jet is highly polarized ($m = 8$ per cent), and by comparison with the 15-GHz image of van Breugel et al. (1992) has a rotation measure (RM) of at least 450 rad m^{-2}. Taylor, Ge & O'Dea (1995) have mapped the RM of this source at 0.4-arcsec resolution, and find an overall RM for the core/jet of 600 rad m^{-2}.

3C 237. The MERLIN image shows a central component and a faint jet between this and the eastern lobe. The unusual 'tongue' of emission to the south of the western lobe is seen to a lesser extent in the VLBI map of Fanti et al. (1985), as is the 'triangular' substructure in the eastern lobe. The distribution of polarized emission in this source is very patchy, and the degree of polarization is also low at 8.4 GHz (Akujor & Garrington 1995), but slightly higher at

Table 2. Component parameters of the CSS sample, measured from the MERLIN 5-GHz images.

Name	Ident.	S_I mJy	S_{pk} mJy/beam	m per cent	χ deg
3C 43	Total	1164			
	A	215	61	4.8	−81
	B	476	319	3.4	3
	C	240	186	3.6	−4
	Jet	206	8	<0.3	
	north	62	2	<0.4	
3C 48	Total	5662		2.2	−87
	south	1480	708	0.9	76
	north	3345	822	4.7	−85
3C 49	Total	976			
	Core	7	7	<4.0	
	east	189	50	<0.3	
	west	776	719	<0.3	
3C 67	Total	856			
	north	342	23	8.0	58
	south	510	126	<0.3	
3C 93.1	Total	652	199	0.4	85
	'Core'	321	199	0.6	−72
	'Jet'	142	128	0.6	−53
3C 119	Total	4384	3035	0.9	65
	Peak		3035	0.8	72
3C 138	Total	3340	109		
	Core	460	329	<0.3	
	Jet	2684	1095	12	−11
	east	125	50	<0.3	
3C 147	Total	7456			
	core	2500	2276	0.6	9
	Jet	6191	1310	<0.3	
	north	740	112	<0.3	
3C 186	Total	228			
	Core	15	14	<2.0	
	Jet	93	19	<1.5	
	south	90	32	<1.0	
3C 190	Total	658			
	north	156	55	<0.3	
	Core	73	65	<0.3	
	Jet	381	59	<0.3	
3C 216	Total	913			
	Core	736	670	1	69
	Jet	201	124	7.6	55
3C 237	Total	1962			
	east	868	235	1.4	74
	Core		4		
	west	1227	271	0.7	−16
3C 241	Total	303	106		
	west	201	106	<0.3	
	Core	3	3		
	east	92	57	<0.3	
3C 258	Total	376			
	north	163	137	<0.3	
	south	250	206	<0.3	
3C 268.3	Total	1054			
	north	673	161	<0.3	
	south	381	34	5.8	83
3C 277.1	Total	742			
	south	416	173	<0.9	
	Core		46.2	<1.0	
	north	255	25	6.2	−3
3C 286	Total	7160	5351	11.3	33
	Peak		5351	11.2	36
3C 298	Total	1345			

Table 2 – *continued*

Name	Ident.	S_I mJy	S_{pk} mJy/beam	m per cent	χ deg
	east	507	98	3.7	−26
	Jet		174	101	<2.0
	Core	311	281	2.0	77
	west	345	170	<1.5	
3C 303.1	Total	333			
	north	24	3	3.0	−72
	south	308	91	1.0	43
3C 305.1	Total	320			
	south	86	7	< 4.5	
	north	233	44	1.1	49
3C 309.1	Total	2848			
	west	109	12		
	Core	2163	1690	5.2	44
	Jet	146	22	7.1	−57
	Head	483	83	5	−77
3C 318	Total	777			
	Core	22	15	1.0	
	Jet	540	289	3.6	44
	Lobe	212	83	<0.3	
3C 343	Total	1434	423	0.8	70
3C 343.1	Total	1152			
	east	368	178	<0.9	
	west	785	383	<0.6	
3C 380	Total	4250			
	Core	3196	3045	5.8	42
	A	382	223	2.9	−24
	B	446	47	16.0	−54
	C	95	20	31.2	−52
3C 454	Total	813			
	A	336	272	13.8	−34
	B	262	164	5.8	45
	C	76	64	4.0	67
	D	38	15	3.2	2
	Lobe	83	23	0.4	69
3C 454.1	Total	247	97	< 0.5	
	south	76	39	<1.6	
	north	171	97	<0.6	
4C 13.66	Total	279	88		
	north	31	18	<5.0	
	south	243	88	<1.0	

15 GHz (van Breugel et al. 1992). This suggests that the lobes are almost completely depolarized at 5 GHz, except for a few patches where the distribution of Faraday rotation may be more coherent.

3C 241. We confirm that the central component at $10^{\rm h}19^{\rm m}09\overset{\rm s}{.}368$, $22°14'39\overset{''}{.}73$ is indeed the flat-spectrum core in this small radio galaxy by comparison with the 15-GHz map of van Breugel et al. (1992). No polarization is detected at 5 or 15 GHz in this source.

3C 258. The MERLIN 5-GHz image just resolves this source into two components. A VLBI image at 1.6 GHz (Sanghera et al. 1995) shows that both are extended, and a comparison of the flux densities gives spectral indices of 0.32 and 0.56 for the southern and northern components, respectively. No polarization is detected in this source. Lower resolution WSRT maps (Strom et al. 1990) show faint emission extending approximately 1 arcmin to the north and south. This source should properly be classified as a steep-spectrum core source.

3C 268.3. This radio galaxy is quite asymmetric in both radio structure and polarization. As in 3C 67, only the fainter, more diffuse component is strongly polarized at 5 GHz. At higher frequencies, this lobe shows steadily higher polarization (Akujor & Garrington 1995), whereas the northern lobe remains unpolarized. A weak, unresolved component at $12^{\rm h}03^{\rm m}54\overset{\rm s}{.}096$, $64°30'18\overset{''}{.}68$, which may be the core, is detected 0.3 arcsec south of the northern hotspot, but further observations are required to confirm this.

3C 277.1. The MERLIN image shows for the first time a knotty jet linking the core to the north-west component, and confirms the 'Z'-shaped distortion of the south-east component seen in the VLBI map of Sanghera et al. (1995). This source shows a striking polarization asymmetry at 5 GHz: the polarization reaches 10 per cent on the jet side, but is undetectable (< 1 per cent) on the counter-jet side.

3C 286. The MERLIN 5-GHz image presented here shows only the central steep-spectrum 'core' of this quasar. The fainter component to the east and the jet to the south-west (e.g. Akujor & Garrington 1995) were detected, but only at a low signal-to-noise ratio, and are not shown here. EVN observations (Jiang et al. 1996)

show that the polarization E-vectors follow the inner part of this jet. The MERLIN map shows that the jet begins to twist to the west, and that the polarization direction changes at this point. From the MERLIN+EVN map of Jiang et al., this also corresponds to a break in the jet or lobe.

3C 298. The MERLIN image reveals a continuous jet between the core and the eastern hotspot. Only the outer part of this jet is polarized, suggesting a strong gradient in the degree of depolarization.

3C 303.1. The two lobes of this radio galaxy have similar morphologies, but differ in flux density by a factor of 10. There is as yet no evidence for a core in this source. The northern component appears quite highly polarized (up to 20 per cent at its tip), whereas the brighter southern component shows at most 1 per cent polarization.

3C 305.1. The MERLIN image shows that the northern component consists of a knotty jet with more diffuse emission extending to the west, and a ring-like southern lobe. The knot at the southern end of the jet has a spectral index of 0.6, and is highly polarized at 15 GHz (van Breugel et al. 1992). This component is therefore unlikely to be the core. The only detection of polarized emission in the MERLIN 5-GHz map is at the tip of the northern component. However, at this resolution the limit on the fractional polarization over most of the source is only 6 per cent. Even so, there appears to be significant depolarization between 5 and 15 GHz.

3C 309.1. The MERLIN 5-GHz image shown here is very similar to the EVN+MERLIN image at 1.6 GHz of Wilkinson et al. (1986). The jet and eastern lobe are quite highly polarized, and the way in which the magnetic field appears to follow the boundary of the lobe implies low Faraday rotation there. Along the jet, there is more variation in the polarization direction, either because of complex structure within the jet or because of Faraday rotation.

3C 318. The MERLIN 5-GHz image suggests that this source has a weak core with a one-sided jet to the north-east and an extended lobe to the south-west. The core might be identified with knot k1 of Spencer et al. (1991), but in that map it appears resolved and does not have a particularly flat spectrum.

3C 343. VLBI observations of this source reveal a complex distorted radio structure, which is barely resolved in the MERLIN image presented here. Only the eastern extension shows significant polarization (1 to 5 per cent).

3C 343.1. The MERLIN image confirms the basic double structure of this source. No polarization above 1 per cent was detected.

3C 380. The multifrequency polarization properties of this source have been studied by Flatters (1987) and Wilkinson et al. (1991) with the VLA and MERLIN. The unresolved southernmost component in our map contains the core and the VLBI jet, which has 6 per cent polarized emission, with position angles perpendicular to the jet. In the component B, m is 16 per cent and the position angles are parallel to the original jet direction. We have partially resolved the region where the jet appears to be disrupted, changing direction towards the east, possibly creating the arc seen by Flatters.

3C 454. This source has a jet lying along the north–south direction. Comparison with the MERLIN+EVN at 1.6 GHz (Spencer et al. 1991) suggests that the component marked C may have a flatter spectrum, and may contain the core, but higher resolution observations are required to confirm this. The jet components (B and C) are about 5 per cent polarized.

3C 454.1. This source appears as a simple double with no core detected above 0.5 mJy. The individual components are barely resolved and unpolarized at 5 GHz. This source was observed as part of a separate project and the map will be published elsewhere (Law-Green et al., in preparation).

4C 13.66. This was the final source to be identified in the revised 3C sample, and has been discussed in detail by Rawlings et al. (1996). The MERLIN 5-GHz image was observed as part of this programme, and the map is reproduced here for completeness. No polarization is detected at 5 GHz.

4 DISCUSSION

The new MERLIN 5-GHz maps at 60-mas resolution show details of the structures of these sources hitherto only suggested by lower dynamic range VLBI studies. Jets are more pronounced in the quasars than in the radio galaxies (Spencer et al. 1991); indeed, all of the quasars in the present sample have one-sided jets. The new maps show a wide variety of jet structures, from the highly curved jet of 3C 43 to the remarkably straight and smooth jet of 3C 186. The MERLIN images are ideally suited in resolution and sensitivity to searching for the weaker jets in radio galaxies. The present sample contains 13 radio galaxies, of which three have jets (3C 49, 305.1 and 318), and three have linear features which may be jets running through their lobes (3C 67, 237 and 268.3). Using MERLIN and the EVN, we can now resolve the lobes of CSS radio galaxies and quasars into the sort of structure commonly seen in more extended sources.

The polarization of the CSS sources in this sample at 5 GHz is generally low: in 13/27 sources, the extended emission is unpolarized (< 2 per cent) and in a further nine sources one of the two lobes is unpolarized. Overall, the median fractional polarization is $\lesssim 2$ per cent (excluding flat-spectrum core components). Similar results have been found at much lower resolution at this frequency for different samples of CSS sources by van Breugel, Miley & Heckman (1984), Saikia, Kodali & Swarup (1985) and Akujor & Garrington (1995). For comparison, extended sources have typical polarization of 5–15 per cent, with less than 3 per cent of the components being unpolarized at this frequency (Garrington, Conway & Leahy 1991). A few components are more highly polarized, e.g., the jets in 3C 309.1, 138, 216 and 43 and the more extended lobes of 3C 67 and 268.3.

There are two possible explanations for the low polarization: an intrinsic effect, perhaps due to highly tangled magnetic fields within the components, or Faraday depolarization, either within the radio lobes or by thermal gas surrounding the sources. Given the high resolution of the present maps, the magnetic field structures should be well resolved, but several of the larger components (e.g., 3C 49W, 67S, 147N and 186) are unpolarized. The field tangling scale may well scale with the source (or lobe) size, but the present maps are comparable to those of Garrington et al. (1991) in terms of the ratio of resolution to source size.

We believe that the low polarization is due to Faraday depolarization. Except for three sources (3C 258, 3C 454 and 4C 13.66), all the sources studied here have been observed at 8.4 and 15 GHz using the VLA with a resolution of about 0.2 arcsec (van Breugel et al. 1992; Akujor & Garrington 1995; Garrington & Akujor 1996). Because of the difference in resolution between the MERLIN and VLA data, we cannot derive accurate values for the depolarization ratio between 15 and 5 GHz, but the following conclusions can be drawn. Of the 13 sources which were found to be unpolarized with MERLIN at 5 GHz, four are also unpolarized at 15 GHz, and six have significantly higher polarization in one or more components at 15 GHz. In the nine sources where just one component is

unpolarized, there is evidence for higher polarization at higher frequencies in four sources. Significant depolarization between 15 and 5 GHz is also seen in the polarized lobes of 3C 318 and 268.3. We stress that since the observations at the higher frequencies are at lower resolution, the depolarization must be a function of frequency and not of resolution. We conclude that there is evidence for Faraday depolarization between 5 and 15 GHz in several of the CSS sources studied here, and suggest that those with low polarization at 15 GHz are the most extreme cases. Observations at 22 GHz are needed to confirm this, and are currently underway.

Faraday depolarization is often quantified by $\lambda_{1/2}$, the wavelength at which the fractional polarization has fallen to half its zero-wavelength value. For the majority of CSS source components $\lambda_{1/2} < 0.06$ m, and for several of these we believe that $\lambda_{1/2} < 0.02$ m. Assuming a Gaussian distribution of the fluctuations in Faraday depth ($\phi = \int n_e \mathbf{B}\cdot \mathrm{d}\mathbf{l}$ cm^{-3} μG pc; Burn 1966), the rms value, or Faraday dispersion, is

$$\Delta = 0.74(1+z)^2/\lambda_{1/2}^2 \text{ cm-3 } \mu\text{G pc} \quad . \tag{1}$$

For the low-polarization CSS sources we estimate $\Delta \gtrsim 10^3$ cm^{-3}G pc. This is comparable to the high Faraday rotation measures seen in several CSS sources (Taylor, Ionue & Tabara 1992).

The gas responsible for the Faraday rotation is probably associated with the hot ISM of the host galaxy as seen in X-ray emission (Fabbiano 1989). Cooler, denser material revealed by optical narrow-line emission (e.g. McCarthy, Spinrad & van Breugel 1995) may produce very high Faraday depths on small scales, but since the covering factor of this gas is probably low, it will not produce significant depolarization. In the hot gas, the spatial fluctuations in Faraday rotation are probably due to tangling of the magnetic field, and the Faraday dispersion is approximately

$$\Delta = n_e B (Ld)^{1/2} \text{ cm}^{-3}\ \mu\text{G pc}, \tag{3}$$

where n_e and B are the rms values of the electron density and magnetic field strength, L is the path-length through the gas, and d is the tangling scale of the magnetic field.

The fact that depolarization is pronounced in the high-resolution MERLIN images means that the fluctuations must be occurring on scales comparable to or smaller than the beamwidth, i.e., $d \lesssim 100$ pc (at a redshift $z = 1$). This is considerably smaller that the limit set by previous VLA observations of both large (Johnson, Leahy & Garrington 1994) and small sources (Perley & Taylor 1990).

Several of the sources show pronounced asymmetry in the polarization of the two lobes at 5 GHz (3C 67, 138, 268.3, 277.1, 298, 303.1 and 318). All but one of these sources (3C 303.1) have one-sided jets or candidate jets, and in all cases the polarization at 5 GHz is stronger on the side with the jet. We attribute this polarization asymmetry to an asymmetry in depolarization, as seen in more extended sources (Laing 1988; Garrington et al. 1988, 1991), but at higher frequencies in the CSS sources. This is consistent with the depolarization occurring in a surrounding halo, with a size comparable to that of the source. The depolarization is weaker; hence the 5 GHz polarization is stronger, in the nearer of the two lobes. If the kpc-scale jets are relativistic, this lobe will have the brighter jet. Radio galaxies also show a tendency for the lobe closer to the nucleus to depolarize more strongly (e.g. Garrington & Conway 1991). This may be the result of a large-scale asymmetry in the distribution of gas surrounding the radio source, or simply the consequence of a radial decline in the gas density on these scales. Based on the core identifications discussed above, this effect may contribute to the pronounced polarization asymmetry seen in 3C 67 and 268.3. The asymmetric depolarization implies that the path-length through the gas is not much larger than the source size. For a typical path-length of 10 kpc we estimate $nB \sim 1$ cm^{-3}μG, which, for a typical interstellar magnetic field strength of 1 μG, gives $n_e \sim 1$ cm^{-3}, comparable to the density required to confine the narrow-line clouds (Bremer et al. 1992). This density is much higher than that inferred from polarization measurements of more extended sources, and would be consistent with a steady radial decline in the ambient density over scales of 1–100 kpc. Models of the evolution of radio sources from CSS sources to more extended sources require just such a density profile (Fanti et al. 1995; Readhead et al. 1996).

5 CONCLUSIONS

The upgraded MERLIN array has been used to produce total intensity and polarization images of a sample of 28 compact steep-spectrum sources. With an angular resolution of ∼60 mas and rms noise levels of down to 0.1 mJy beam^{-1}, these are amongst the most detailed polarization images of CSS sources available. This combination of resolution and sensitivity is ideal for studying the structure of CSS sources. The new images have confirmed the suspected location of the radio nuclei in several sources, and have revealed one-sided radio jets in 3C 49 and 277.1.

The most highly polarized components are the jets of some of the CSS quasars, and the more extended lobes of two of the radio galaxies. The magnetic field configurations are as expected from the larger sources: mostly parallel to the jets and circumferential in the radio lobes.

However, the most striking feature of the polarization images is the fact that at least 30 per cent of the extended components are unpolarized, with limits to the degree of polarization as low as 0.3 per cent in most cases. Comparison with published data at 8.4 and 15 GHz implies that the low polarization at 5 GHz is due to Faraday depolarization. VLA observations at 22 GHz with similar resolution to the MERLIN 5-GHz images are underway, and should provide accurate values of the depolarization ratio. From the comparison with existing data, we estimate that the Faraday dispersion for the unpolarized sources is at least 1000 cm^{-3} μG pc, at least an order of magnitude higher that in the more extended sources. If this depolarization is due to spatial variation in Faraday rotation in the ISM of the host galaxies, we estimate typical densities of 1 cm^{-3} for a magnetic field strength of 1 μG. The high resolution of the MERLIN observations implies that the magnetic field is tangled on very small scales – less than about 100 pc.

ACKNOWLEDGMENTS

We thank the referee for his very useful and detailed comments on an earlier draft of this paper. EL acknowledges the Brazilian agency CNPQ for a fellowship, CAPES for his PhD scholarship at NRAL, the CVCP/UK for an ORS award, and the NRAO/AOC personnel for their hospitality. The Very Large Array is a national facility operated by the NRAO on behalf of the NSF. MERLIN is a national facility operated by the University of Manchester on behalf of PPARC.

REFERENCES

Akujor C. E., Garrington S. T., 1995, A&AS, 112, 235
Akujor C. E., Spencer R. E., Wilkinson P. N., 1990, MNRAS, 244, 362

Akujor C. E., Spencer R. E., Saikia D. J., 1991, A&A, 249, 337
Akujor C. E., Spencer R. E., Zhang F. J., Fanti C., Lüdke E., Garrington S. T., 1993, A&A, 274, 752
Baars J. W.M, Genzel R., Paulini-Toth I. I. K., Witzel A., 1977, A&A, 61, 99
Bignell R. C., Perley R. A., 1985, in Perley R. A., Schwab F. R., Bridle A. H., eds, Proc. NRAO Summer School on Synthesis Imaging. NRAO, p. 49
Bremer M. N., Crawford C. S., Fabian A. C., Johnstone R. M., 1992, MNRAS, 254, 614
Burn B. J., 1966, MNRAS, 133, 67
Conway R. G., Kronberg P. P., 1969, MNRAS, 142, 11
Dallacasa D. et al., 1990, in Fanti R., Fanti C., O'Dea C. P., Schilizzi R. T., eds, Proc. of the Dwingeloo Workshop on Compact Steep Spectrum and Gigahertz Peaked Spectrum Sources. Istituto di Radioastronomia, Bologna, p. 77
Dallacasa D., Cotton W., Fanti C., Fanti R., Foley A. R., Schilizzi R. T., Spencer R. E., 1995, A&A, 299, 671
Fabbiano G., 1989, ARA&A, 27, 87
Fanti C., Fanti R., Parma P., Schilizzi R. T., van Breugel W. J. M., 1985, A&A, 143, 292
Fanti C., Fanti R., Dallacasa D., Schilizzi R. T., Spencer R. E., Stanghellini C., 1995, A&A, 302, 317
Fanti R., Fanti C., Schilizzi R. T., Spencer R. E., Nan Rendong, Parma P., van Breugel W. J. M., Venturi T., 1990, A&A, 231, 333
Fejes I., Porcas R. W., Akujor C. E., 1992, A&A, 257, 459
Flatters C., 1987, Nat, 326, 683
Flatters C., Conway R. G., 1985, Nat, 314, 425
Garrington S. T., Akujor C. E., 1996, in Ekers R. et al., eds, Proc. IAU Symp. 175, Extragalactic Radio Sources. Kluwer, Dordrecht, p. 77
Garrington S.T, Conway R. G., 1991, MNRAS, 250, 198
Garrington S.T, Leahy J.P, Conway R.G, Laing R.A, 1988, Nat, 331, 147
Garrington S.T, Conway R.G, Leahy J.P, 1991, MNRAS, 250, 171
Jenkins C. J., Pooley G. G., Riley J. M., 1977, Mem. RAS, 84, 61
Jiang D. R., Dallacasa D., Schilizzi R. T., Luedke E., Sanghera H. S., Cotton W. D., 1996, A&A, 312, 380
Johnson R. A., Leahy J. P., Garrington S. T., 1995, MNRAS, 273, 877
Laing R. A., 1988, Nat, 331, 149
Laing R. A., Riley J. M., Longair M. S., 1983, MNRAS, 204, 151
Lüdke E., 1994, PhD thesis, Univ. Manchester
McCarthy P. J., Spinrad H., van Breugel W., 1995, ApJS, 99,27
Patnaik A. R., Browne I. W. A., Wilkinson P. N., Wrobel J. M., 1992, MNRAS, 254, 655
Pearson T. J., Readhead A. C. S., Perley R. A., 1985, AJ, 90, 738
Perley R. A., Taylor G. B., 1991, AJ, 101, 1623
Rawlings S., Lacy M., Leahy J. P., Garrington S. T., Lüdke E., 1996, MNRAS, 279, 13
Readhead A. C. S., Taylor G. B., Xu W., Pearson T. J., Wilkinson P. N., Polatidis A. G., 1996, ApJ, 460, 612
Rendong Nan., Schilizzi R. T., Fanti C., Fanti R., Muxlow T. W. B., Spencer R. E., 1991, A&A, 245, 449
Saikia D. J., Kodali P. D., Swarup G., 1985, MNRAS, 216, 385
Sanghera H. S., Saikia D. J., Lüdke E., Spencer R. E., Foulsham P. A., Akujor C. E., Tzoumis A. K., 1995, A&A, 295, 629
Spencer R. E. et al., 1991, MNRAS, 250, 225
Strom R. G., Riley J. M., Spinrad H., van Breugel W. J. M., Djorgivski S., Liebert J., McCarthy P. J., 1990, A&A, 227, 19
Taylor G. B., Ionue M., Tabara H., 1992, A&A, 264, 421
Taylor G. B., Ge J., O'Dea C. P., 1995, AJ, 110, 522
Thomasson P.T, 1986, QJRAS, 27, 413
Wilkinson P.N, 1991, in Cornwell T. J., Perley R. A., eds, Proc. IAU Colloq. 131, Radio Interferometry: Theory, Techniques and Applications. Astron. Soc. Pac., San Francisco, p. 381
Wilkinson P. N., Kus A. J., Pearson T. J. Readhead A. C. S., Cornwell T. J., 1986, in Swarup G., Kapahi V. K., Proc IAU Symp. 119, Quasars. Reidel, Dordrecht, p. 165
Wilkinson P. N., Akujor C. E., Cornwell T. J., Saikia D. J., 1991, MNRAS, 248, 86
van Breugel W. J. M., Miley G. K., Heckman T., 1984, AJ, 89, 5
van Breugel W. J. M., Fanti C., Fanti R., Stanghellini C., Schilizzi R. T., Spencer R. E., 1992, A&A, 256, 56
Zhang F. J., Akujor C. E., Chu H. S., Mutel R. L., Spencer R. E., Wilkinson P. N., Alef W., Matveyenko L. I., Preuss E., 1991, MNRAS, 250, 650

This paper has been typeset from a $\TeX$/$\LaTeX$ file prepared by the author.